Sliding Modes Differentiators with Dynamic Gains for Edge Detection Processing

Lilia Sidhom, Mohamed Smaoui, Xavier Brun, Eric Bideaux

International Journal of Innovative Computing, Information and Control
Volume **13**, Number **2**, April **2017**

ICIC International ©2017 ISSN 1349-4198
pp. 381–396

SLIDING MODES DIFFERENTIATORS WITH DYNAMIC GAINS FOR EDGE DETECTION PROCESSING

Lilia Sidhom[1], Mohamed Smaoui[2], Xavier Brun[2] and Eric Bideaux[2]

[1]Electrical Engineering Department
University of Tunis El Manar-ENIT-LARA
BP 37, Le Belvédère, 1002 Tunis, Tunisie
lilia.sidhom@gmail.com

[2]AMPERE UMR 5005 Laborator, INSA Lyon
20 Avenue Albert Einstein, 69100 Villeurbanne, France
{ Mohamed.smoaui; xavier.brun; eric.bideaux }@insa-lyon.fr

Received September 2016; revised January 2017

Abstract. *The basic idea of this paper is to introduce dynamic gains in the classic sliding modes differentiators to ameliorate their performance mainly according to noise reduction on the estimated signals. New schemes of 1st and 2nd-order sliding modes differentiators are proposed which satisfy some convergence properties. The originality of this paper is to apply the proposed algorithms to both estimating the derivatives of mono-dimensional and two-dimensional noisy signals. Their effectiveness is illustrated via simulation tests where these algorithms are used as an edge detector into image application. A comparative study with conventional approaches is then performed.*
Keywords: Differentiator design, Dynamic gains, Edge detection, Higher order sliding modes, Image application, Comparative study

1. **Introduction.** The major problem of noisy differentiation signal is the amplification of the noises on the signal estimation. This problem becomes more important in practice where the measurement noises are not obvious to model. Then it is so hard to discern between the noise and the basic signal. Thus, the practical differentiation consists of a trade-off between exact differentiation and robustness with respect to noises.

In the literature, two major approaches are basically proposed to estimate the noisy signal derivatives. For the first one, the problem of noisy derivative estimation is addressed by an observation and a filtering problem. In this case, the knowledge of the system and/or noise models is necessary. For example, in the stochastic case, the Kalman filter [2] can be used to estimate a derivative of some noisy signal. However, the computing of the gain-filter requires the resolution of an algebraic Ricatti equation. In [1], the authors estimate the derivative of signal using a high gain observer. The main drawback of this last one is its sensitivity to measurement noises due to its parameter setting. For the nonlinear case, we can cite: backstepping observer [3], sliding mode observers [4].

Unfortunately, in many cases the lack of information about the system dynamics and unknown features about the noise, makes the design of differentiator unavoidable. Rather than the model approach, the differentiator approach can be then considered. The traditional method is the finite difference method such as the Euler backward difference method. This one is simple to implement in real time, but in the presence of noise, it presents bad noise suppression capabilities. To avoid this problem, a low-pass filter can be used to attenuate the noise but with introducing an inevitable phase delay. Other more attractive methods exist in the literature. One of them is based on the truncated Taylor

series of the signal to differentiate [6]. Despite of good filtering results, the algebraic algorithms are sensitive to the truncation order, to the size of the sliding window estimation and the setting of its parameters. Alternative methods based on the sliding mode technique can be employed. In [7], the author proposes an arbitrary-order differentiator with finite-time convergence. One of the most popular is super-twisting (ST) differentiator [7]. The advantages of such differentiators are the easiness of its implementation and their finite-time robust differentiation of bounded noisy signals. However, the major problem of such differentiator concerns the tuning of its gains to match convergence and good accuracy. In fact, the algorithm parameters depend on the Lipschitz constant of the derivative signal. In real time, this constant is usually not exactly known beforehand. Thus, other new forms of 1st-order sliding modes differentiator (ST) have been developed to avoid the drawback of the classic one, such in [12,13]. Other new forms of the ST differentiator were successfully applied in [5,14]. This work is an extension of that shown in [5] with a modification in the convergence proof of the proposed algorithms.

In this work, we are looking for a differentiator design with basing on the higher order sliding modes. Our contributions are summarized as follows: (i) new scheme of the ST algorithm is proposed different from those presented in the literature; (ii) new scheme of 2nd-order differentiator is based on three-order sliding modes. As far as we know, the proposed sliding modes algorithms will yield to the first image processing application, especially for edge detection. In fact, the defined differentiators can be used to compute respectively the gradient and/or the Laplacian of image in order to obtain the edge. Despite the most commonly using of the differential edge detection schemes [8], these detectors suffer from their sensitivity to noise. Furthermore, for such scheme, the sizes of the kernel and coefficients filter are fixed and cannot be adapted to a given image. The noise derivative can mask the real maxima that indicate edges. To overcome this drawback, other methods are developed in the literature, such as Canny filter [9]. Interesting works can be cited for the edge detector context as [12,13].

This paper is organized as follows. In the second section, a problem statement is exposed and the new schemes of sliding modes differentiators are presented. Section 3 shows some simulation results to compare these new schemes with the classic one, in the mono-dimensional (1D) context. Section 4 is dedicated to implementing the proposed schemes for edge detection. A comparative study will be then presented with classic edge detectors. Finally, Section 5 concludes this paper.

2. **Problem Statement.**

2.1. **Problem statement.**

As well as when applied to designing controller, the sliding modes technique shows good results when used for robust differentiation [7]. It is also the case for the ST algorithm [11]. To design a sliding modes differentiator, let the input signal $f(t)$ to be differentiated, be a function defined on $[0, +\infty)$ and be measurable in Lebesgue's sense. This signal is considered as the sum of the two following terms:

$$f(t) = f_0(t) + \xi(t) \tag{1}$$

where $f_0(t)$ is an unknown base signal for which the $(n+1)$th derivative has a known Lipschitz constant $C \succ 0$, and $\xi(t)$ is a bounded Lebesgue-measurable noise with unknown features, defined by: $|\xi(t)| < \varepsilon$, with ε sufficiently small ($\varepsilon << 1$).

An infinite number of differentiator schemes is proposed in [7] and aims at the calculation in real time of $\dot{f}_0(t), \ddot{f}_0(t), \ldots, f_0^{(n)}(t)$. These schemes are defined in (2), where λ_i, $i \in \{0, \ldots, n\}$ are positive gains depending on the Lipschitz constant C of $f_0^{(n+1)}(t)$. The outputs of the differentiator are defined by $z_i = v_{i-1}$ which are the estimation of

$f^{(i)}(t)$, $i \in \{1,\dots,n\}$. From (2), the ST algorithm ($n=1$) and the 2nd-order differentiator ($n=2$) can be easily defined. Thus, the initial value $z_0(0)=f(0)$, $z_i(0)=v_{i-1}(0)$ with $i \in \{1,\dots,n\}$ are chosen according to desired time of convergence. The parameters λ_i can be chosen as:

$$\lambda_i = \lambda_{i0} C^{\frac{1}{n-i+1}} \tag{2}$$

From (2), the choice of the coefficient set is such that $\lambda_{00} < \lambda_{10} < \cdots < \lambda_{n0}$. So, the choice of these gains is conditioned by the knowledge of the constant C. Then with the same tuning gains, a simple modification of the spectral content of the input signal or of its magnitude can greatly affect the estimation of the derivative. Generally, the gain values are found by guessing with computer simulations.

$$\begin{cases} \dot{z}_0 = v_0 \\ v_0 = -\lambda_0 |z_0 - f|^{\frac{n}{n+1}} sign(z_0 - f) + z_1 \\ \dot{z}_1 = v_1 \\ v_1 = -\lambda_1 |z_1 - v_0|^{\frac{n-1}{n}} sign(z_1 - v_0) + z_2 \\ \quad \vdots \\ \dot{z}_{n-1} = v_{n-1} \\ v_{n-1} = -\lambda_{n-1} |z_{n-1} - v_{n-2}|^{\frac{1}{2}} sign(z_{n-1} - v_{n-2}) + z_n \\ \dot{z}_n = -\lambda_n sign(z_n - v_{n-1}) = -\lambda_n sign(z_{n-1} - v_{n-2}) \end{cases} \tag{3}$$

From the theoretical sliding mode, the first term of all the equations in (3) must be equal to zero. However, it is impossible in practice to cancel these terms due to different present sources of inaccuracy. Indeed, the presence of the "*sign*" function in these terms leads also to oscillations at high frequencies. This chattering effect can deteriorate the precision of the outputs differentiator. In the presence of noises, the noise amplification on the estimated signals becomes then even larger. So, it is not easy to set the gains to reach a good compromise between accuracy and robustness to noise.

2.2. **Proposed solution.** To overcome the exposed problem, we propose to add dynamic laws to compute online the parameters of the sliding mode differentiators.

• *New schema of 1st-order differentiator.* The proposed 1st-order differentiator is defined by the following system:

$$\begin{cases} \dot{z}_0 = v_0 \\ v_0 = -\hat{\lambda}_0 |z_0 - f|^{\frac{1}{2}} sign(z_0 - f) - K_0 (z_0 - f) + z_1 \\ \dot{z}_1 = v_1 \\ v_1 = -\hat{\lambda}_1 sign(z_0 - f) \end{cases} \tag{4}$$

The sliding surfaces are given by:

$$\begin{cases} \sigma_0 = z_0 - f \\ \sigma_1 = z_1 - \dot{f} \end{cases} \tag{5}$$

Using the variables defined in (5), the system (4) can be rewritten as follows:

$$\begin{cases} \dot{\sigma}_0 = -\hat{\lambda}_0 |\sigma_0|^{\frac{1}{2}} sign(\sigma_0) - K_0 \sigma_0 \\ \dot{\sigma}_1 = -\hat{\lambda}_1 sign(\sigma_0) \end{cases} \tag{6}$$

Theorem 2.1. *For $K_0 \succ 0$ and with the sliding surfaces defined by (5), all trajectories of algorithm (4) converge at a finite time to the equilibrium point $\sigma_0 = \sigma_1 = 0$, with the dynamic gains $\hat{\lambda}_i$, $i \in \{0, 1\}$ defined by:*

$$\begin{cases} \dot{\hat{\lambda}}_0 = \left(|\lambda_0|^{\frac{1}{2}} \, sign\,(\lambda_0) \right) \lambda_0, \ \hat{\lambda}_0(0) \geq 0 \ \textit{and} \ \dot{\hat{\lambda}}_0 \succ 0, \ \forall t \succ 0 \\ \dot{\hat{\lambda}}_1 = |\lambda_0|\,, \ \hat{\lambda}_1(0) \geq 0 \ \textit{and} \ \dot{\hat{\lambda}}_1 \succ 0, \ \forall t \succ 0 \end{cases} \tag{7}$$

See Appendix A for the proof of the previous theorem.

• *New schema of 2nd-order differentiator.* For the 2nd-order differentiator, three gains $(\lambda_0, \lambda_1, \lambda_2)$ must be adjusted in real time. Let us define now the scheme as:

$$\begin{cases} \dot{z}_0 = v_0 \\ v_0 = -\hat{\lambda}_0 |s_0|^{\frac{2}{3}} sign(s_0) - K_0 s_0 + z_1 \\ \dot{z}_1 = v_1 \\ v_1 = -\hat{\lambda}_1 |s_1|^{\frac{1}{2}} sign(s_1) - \hat{\lambda}_2 \int\limits_0^t sign(s_1) dt - K_1 s_1 \end{cases} \tag{8}$$

K_0 and K_1 are positive gains and s_0, s_1 are the sliding surfaces given by:

$$\begin{cases} s_0 = z_0 - f \\ s_1 = z_1 - v_0 \end{cases} \tag{9}$$

The dynamic gains $\hat{\lambda}_i$, $i \in \{0, 1, 2\}$ are defined by:

$$\begin{cases} \dot{\hat{\lambda}}_0 = \left(|\lambda_0|^{\frac{2}{3}} \, sign(s_0) \right) s_0, \ \hat{\lambda}_0(0) \geq 0 \text{ and } \dot{\hat{\lambda}}_0 \succ 0, \ \forall t \succ 0 \\ \dot{\hat{\lambda}}_1 = \left(|\lambda_0|^{\frac{1}{2}} sign(s_1) \right) s_1, \ \hat{\lambda}_1(0) \geq 0 \text{ and } \dot{\hat{\lambda}}_1 \succ 0, \ \forall t \succ 0 \\ \dot{\hat{\lambda}}_2 = s_1 \int\limits_0^t sign(s_1) dt \end{cases} \tag{10}$$

Theorem 2.2. *For K_0, $K_1 \succ 0$ and with the dynamic gains $\hat{\lambda}_i$, $i \in \{0, 1, 2\}$ defined by (10), the system trajectories (8) converge locally and asymptotically towards the equilibrium point $s_0 = s_1 = 0$ under the following assumption: There are positive constants λ_0^* and λ_1^*, a priori unknown, defined by:*

$$\begin{cases} \dot{f} = -\lambda_0^* |s_0|^{\frac{2}{3}} sign(s_0) + z_1 \\ \ddot{f} = -\lambda_1^* |s_1|^{\frac{1}{2}} sign(s_1) - \lambda_2^* \int\limits_0^T sign(s_1) dt \end{cases} \tag{11}$$

The proof of the previous theorem is in Appendix B.

3. **Simulation Results for 1D Derivative Estimation.** To prove the effectiveness of the proposed schemes compared to classic one, with respect to noise, we perform simulation test which consists of adding to the input signal $f(t)$ a white Gaussian noise with zero mean and standard deviation equal to 0.03.

From Figures 1 and 2, we can notice that the estimate of the 1st-derivative has less noise amplification compared to the estimate of the 2nd-derivative. Then, it is clear that the proposed algorithms have a reduced level of noise compared to the classic versions. This is essentially due to the additional linear component in the output equations. For example, from Figures 1 and 2, the proposed version leads to a noise magnitude 7 times smaller than what is obtained with the classical version. We can conclude that the main advantage of

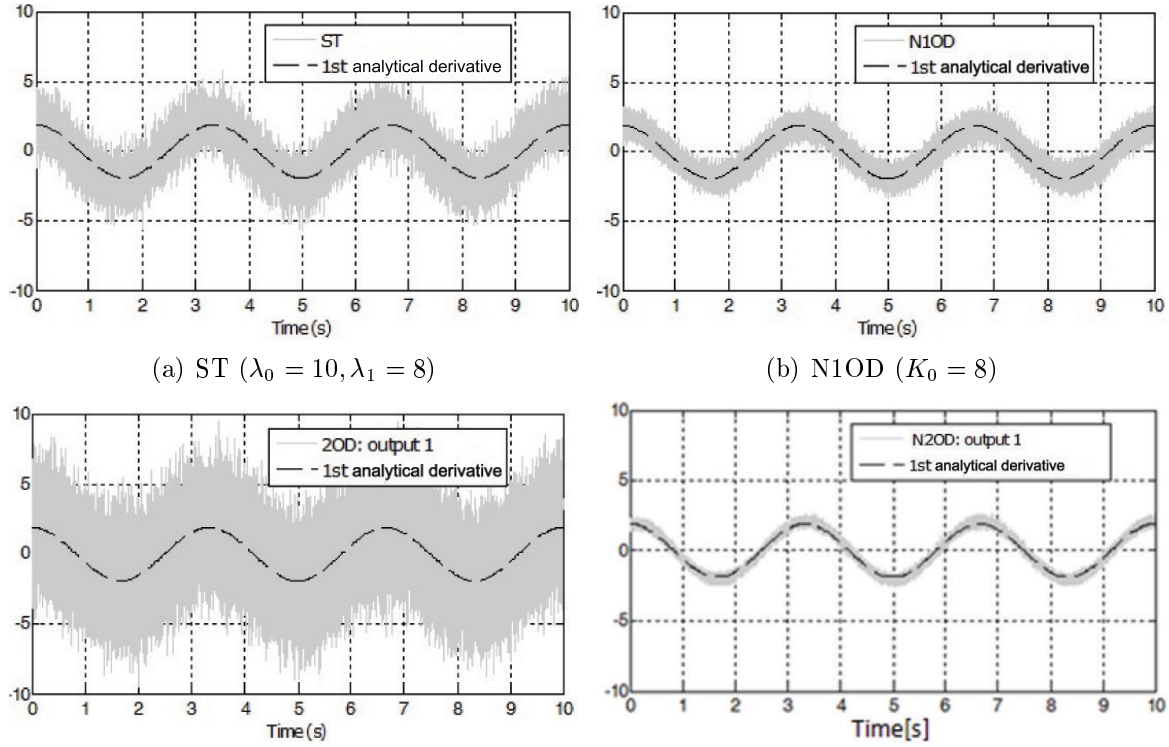

(a) ST ($\lambda_0 = 10, \lambda_1 = 8$) (b) N1OD ($K_0 = 8$)

(c) 2OD ($\lambda_0 = 8, \lambda_1 = 7, \lambda_2 = 3$) (d) N2OD ($K_0 = 7, K_1 = 4$)

FIGURE 1. Estimation of the first derivative

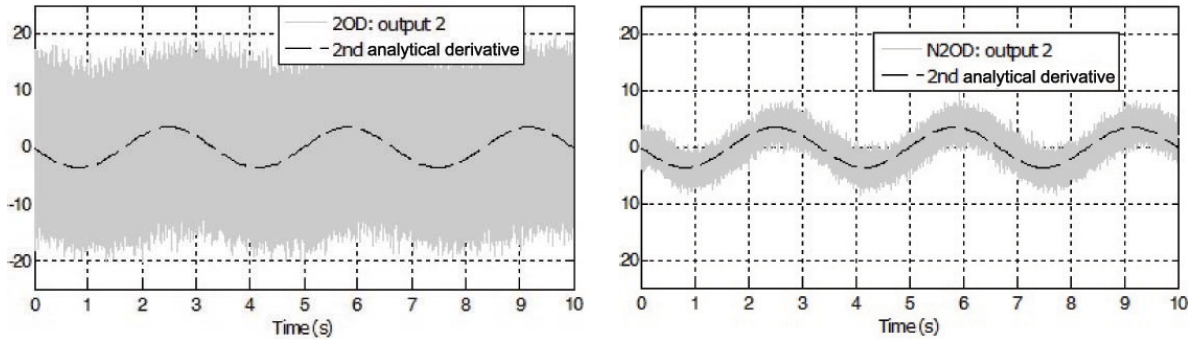

(a) 2OD ($\lambda_0 = 8, \lambda_1 = 7, \lambda_2 = 3$) (b) N2OD ($K_0 = 7, K_1 = 4$)

FIGURE 2. Estimation of the second derivative

the proposed schemas is mainly the noise reduction compared to conventional one. This advantage may be interesting in practice where the presence of noise is unavoidable.

Remarks about the setting of the convergence gains are as follows. (i) For no noisy case: the values of the gains K_i, $i \in \{0, 1\}$ have only effect on the convergence time of the algorithms. In fact, if the convergence gains values are high, the convergence time of the algorithms becomes quick. (ii) For noisy case: there is some compromise between the reduction of the noise amplification on the estimated signals and the convergence time of the differentiators. If very high gain values are taken, the convergence time becomes fast but the noise amplification becomes significant. It is necessary to have low initial values of the dynamic gains to reduce as much as possible the influence of the discontinuous components.

For readability of the figures, we use the following abbreviation: super twisting: ST, 2nd-order differentiator: 2OD, new schema of 1st-order differentiator: N1OD, new schema of 2nd-order differentiator: N2OD.

4. **Simulation Results for 2D Derivative Estimation.** In this paper, only the grey-scale digital images are considered. Let the function $g(x, y)$ be defined in $(\mathbb{R} \times \mathbb{R}) \to \mathbb{R}^+$ where $g(x, y)$ gives the intensity at position (x, y). Since the digital image is represented as a set of discrete pixels, the conventional methods of edge detection perform a 2D spatial gradient computing on an image using a pair of convolution masks.

4.1. **Implementation of the proposed algorithm in 2D domain.** Unlike the convolution methods, the proposed algorithms take as input one pixel at a time. To put the proposed schemes in discrete form, the Euler integration step is applied at each constant sampling interval which is equal to $T_e = 10^{-3}$ second. Then, the discretization schemes of the two proposed differentiators (4) and (8) are given respectively by (12) and (14). So, for the 1st-order differentiator, the discrete form is defined as follows:

$$\begin{cases} z_{0k} = z_{0(k-1)} + T_e\Big[-\hat{\lambda}_{0(k-1)} \left|z_{0(k-1)} - f_{(k-1)}\right|^{\frac{1}{2}} sign\left(z_{0(k-1)} - f_{(k-1)}\right) \\ \qquad -K_0\left(z_{0(k-1)} - f_{(k-1)}\right) + z_{1(k-1)}\Big] \\ z_{1k} = z_{1(k-1)} - T_e\hat{\lambda}_{1(k-1)} sign\left(z_{0(k-1)} - f_{(k-1)}\right) \end{cases} \tag{12}$$

And the equations of dynamic gains take the following discrete forms:

$$\begin{cases} \hat{\lambda}_{0k} = \hat{\lambda}_{0(k-1)} + T_e\left(z_{0(k-1)} - f_{k-1}\right)\left|z_{0(k-1)} - f_{k-1}\right|^{\frac{1}{2}} sign\left(z_{0(k-1)} - f_{k-1}\right) \\ \hat{\lambda}_{1k} = \hat{\lambda}_{1(k-1)} + T_e\left|z_{0(k-1)} - f_{k-1}\right| \end{cases} \tag{13}$$

For the 2nd-order differentiator, we have:

$$\begin{cases} z_{0k} = z_{0(k-1)} + T_e\Big[-\hat{\lambda}_{0(k-1)} \left|z_{0(k-1)} - f_{(k-1)}\right|^{\frac{2}{3}} sign\left(z_{0(k-1)} - f_{(k-1)}\right) \\ \qquad -K_0\left(z_{0(k-1)} - f_{(k-1)}\right) + z_{1(k-1)}\Big] \\ z_{1k} = z_{1(k-1)} - T_e\Big[\hat{\lambda}_{1(k-1)} sign\left(s_{1(k-1)}\right) \\ \qquad -\hat{\lambda}_{2(k-1)}\sum_{k=1}^{kT_e}\frac{T_e}{2}\left(sign\left(s_{1k}\right) + sign\left(s_{1(k-1)}\right)\right) - K_1 s_{1(k-1)}\Big] \end{cases} \tag{14}$$

With $s_{1k} = z_{1(k-1)} - \frac{\left(z_{0k} - z_{0(k-1)}\right)}{T_e}$. The equations of dynamic gains become discrete as follows:

$$\begin{cases} \hat{\lambda}_{0k} = \hat{\lambda}_{0(k-1)} + T_e\left(z_{0(k-1)} - f_{k-1}\right)\left|z_{0(k-1)} - f_{k-1}\right|^{\frac{2}{3}} sign\left(z_{0(k-1)} - f_{k-1}\right) \\ \hat{\lambda}_{1k} = \hat{\lambda}_{1(k-1)} + T_e s_{1(k-1)}\left|s_{1(k-1)}\right|^{\frac{1}{2}} sign\left(s_{1(k-1)}\right) \\ \hat{\lambda}_{2k} = \hat{\lambda}_{2(k-1)} + T_e\left[\sum_{k=1}^{kT_e}\frac{T_e}{2}\left(sign\left(s_{1k}\right) + sign\left(s_{1(k-1)}\right)\right) s_{1(k-1)}\right] \end{cases} \tag{15}$$

The different steps used to estimate the gradient along the rows on the image by the proposed algorithm are given by Figure 3. The first step is to initialize the first pixel intensity value of the matrix g. Then the algorithm starts with a zero estimation error. Afterward, a prediction of the intensity of the next pixel is made by applying the proposed differentiator to approximating the gradient of the corresponding pixel. Then, new value of the error will be considered. All these steps are repeated for each row and column of this matrix. For the 2nd-order algorithm, the computation of the gradient and the Laplacian can be estimated at the same time and they are approximated by the same way

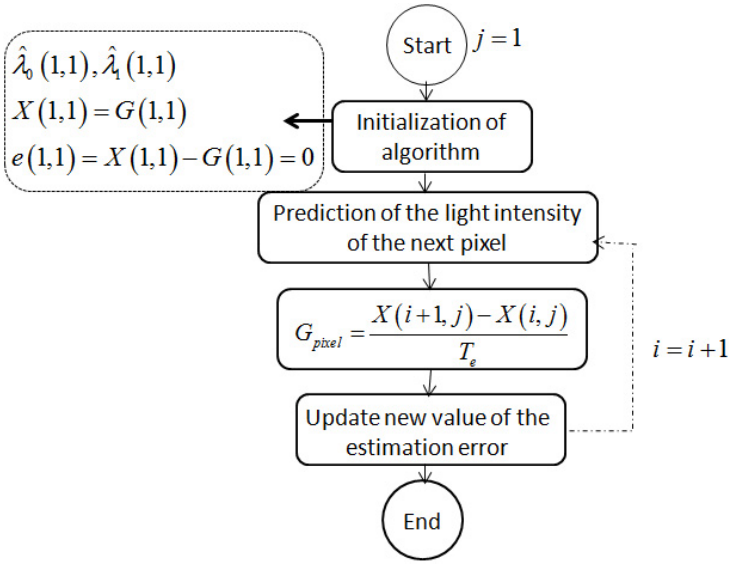

FIGURE 3. Steps to compute the gradient with N1OD along the matrix rows

as the gradient steps. In the case of image, the prediction seems unnecessary because all information can be retrieved directly from the input matrix. However, the idea here is to show the effectiveness of such algorithm for an image in order to extend the work to a frames sequence.

4.2. **Simulation results.** In this section, the proposed schemes are used as an edge detector to compare them with other methods such as the gradient mask, the Prewitt mask and the well-known Canny filter. This last one is widely used as edge detector which has some variable δ to regulate the degree of noise smoothing. The Laplacian operator is used for the second order estimation. To search for the zero crossings of the image, second derivative is calculated with convolving the image with the Laplacian operator. For these all methods, the absolute magnitude of the gradient at each point is approximated by: $|G| = |\nabla g(x,y)| \approx \sqrt{\left(G_x^2 + G_y^2\right)}$, where $G_x = \partial_x(x,y)$ and $G_y = \partial_y(x,y)$ are respectively the vertical and the horizontal gradient of the initial frame.

Methods based on differential operators consist in the use of differentiation to highlight the points with rapid variations of intensity. Thereafter, a step of thresholding must be performed. In order to eliminate insignificant points and to produce the final edge map, we use in our simulation tests, the global thresholding histogram. Note that, in our case, no post-processing will be performed on the simulation results. The goal here is to compare all methods with the same thresholding algorithm.

4.3. **Simulation tests without noise.** The simulation tests have been carried out using MATLAB image processing Toolbox.

In the first time, a standard gray scale image "Lena" (Figure 4(a)) of size (256×256) is selected for simulation study. Firstly, the image is processed without noise. With the N1OD, the vertical and the horizontal gradient (see Figures 4(b) and 4(c)) are estimated with $K_1 = 500$.

The initial values of gains are set to zero. Then, the gradient magnitude is normalized; see Figure 5(a). After thresholding, Figure 5(b) shows the obtained edge. The N2OD is used to estimate the Laplacian relative to the initial image, see Figure 6. In reality, it is very hard to determine the difference between each edge detector, and the obtained

(a) Initial gray image: image 1 (b) G_x of image 1 (c) G_y of image 1

FIGURE 4. Horizontal G_x and vertical G_y gradient of image 1: with N1OD

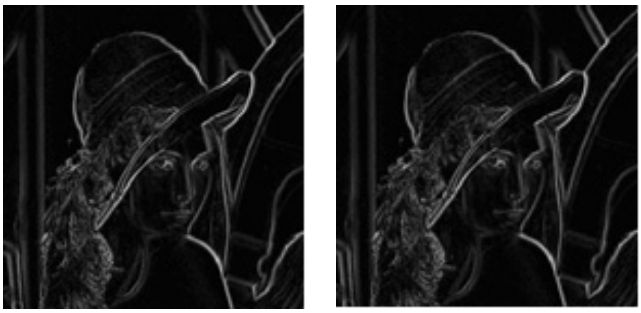

(a) Normalized magnitude of image 1 (b) Normalized magnitude of image 1

FIGURE 5. Edge of image 1: with N1OD

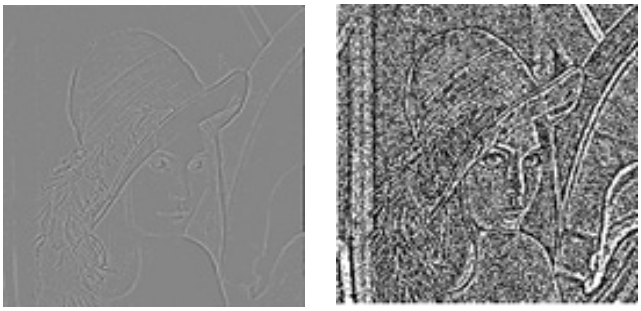

(a) Normalized Laplacian of image 1 (b) Normalized Laplacian after thresholding

FIGURE 6. Edge of image 1: with N2OD

results are relatively the same (see Figure 7). In fact, the absence of the reference edge reveals some difficulties to compare the quality of the results.

4.4. **Simulation tests with noise.** For a given simulation test, a synthetic image (see Figure 8) is used where its edge is exactly known so it is used as a reference for the comparison study. Corrupted image with noise allows us to test the resistance of an edge detector operator to noise. The noise can be described by an additive noise model on the recorded image $i(m, n)$. Consequently, this test image will be corrupted with three different kinds of noise: Gaussian noise which has a zero-mean and is described by its standard deviation σ_n, Salt & Pepper noise which is defined by its density d and Speckle

(a) Gradient operator (b) Prewitt operator (c) Canny filter: $\delta = 0.8$

FIGURE 7. Edge detection by Gradient mask, Prewitt mask and Canny filter

(a) Initial image: test image (b) Exact edge of the test image

FIGURE 8. Test image

noise which is a multiplicative noise as the equation $J = i + n_s i$, where n_s is uniformly distributed random noise with zero-mean and a variance σ_{ns}.

To assess the quality of the obtained edge from the exploited detectors, two kinds of criteria are chosen in our case: qualitative criteria such as complexity of the method, settings parameter and quantitative criteria such as the parameters mean magnitude error (MME), mean edge error (MEE) and the computation time. The MME indicates the average difference of the pixels between the exact magnitude and the estimated one. The MEE represents the error between the exact edge (Figure 8(b)) and the obtained one.

Tests with Gaussian white noise. Upon the simulation tests, the MME and the MEE values are evaluated, for each kind of noise, and are summarized in Tables 1, 2 and 3. The results of edge detection are shown in Figures 10, 12 and 14. It has been observed that the N1OD works well both with the Gaussian, the salt & pepper as well as speckle noise corrupted test image. Especially for the salt & pepper noise, the proposed

TABLE 1. Comparative table of errors: Gaussian white noise

Method	*MME*	*MEE*
Gradient mask	0.0574	0.0038
Prewitt mask	0.0709	0.0128
Canny filter	0.0579	0.0049
N1OD ($K_1 = 400$)	0.0468	0.0024

TABLE 2. Comparative table of errors: salt & pepper noise

Method	*MME*	*MEE*
Gradient mask	0.031	0.0135
Prewitt mask	0.0339	0.0144
Canny filter	0.0124	0.0177
N1OD ($K_1 = 400$)	0.0028	0.0033

TABLE 3. Comparative table of errors: speckle noise

Method	*MME*	*MEE*
Gradient mask	0.0288	0.0019
Prewitt mask	0.0465	0.0157
Canny filter	0.0112	0.000471
N1OD ($K_1 = 400$)	0.0235	0.000261

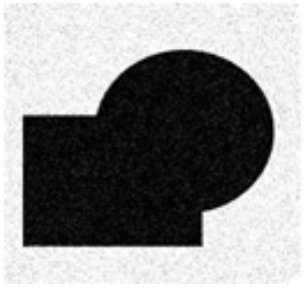

FIGURE 9. Test image corrupted by Gaussian white noise with $\sigma_n = 0.01$

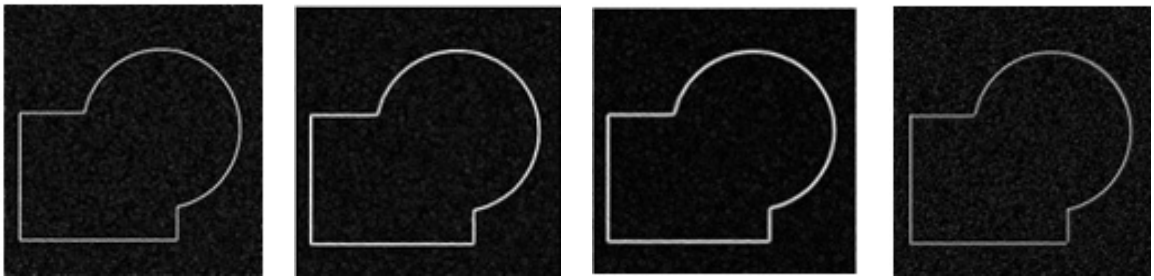

(a) Gradient mask (b) Prewitt mask (c) Canny filter (d) N1OD ($K_1 = 400$)

FIGURE 10. Edge detection of the corrupted image by the Gaussian white noise

algorithm does not amplify the noise in the resulted frame which is not the case for the other methods.

Tests with Salt & Pepper noise. The performance of the gradient mask is better in the presence of speckle noise than the other noises. Indeed, the gradient mask represents a high pass filter so it has not a smoothing action which can explain the amplification of the noise (Figure 12(a)). However, the Prewitt and the Canny filter can estimate the gradient of the input matrix with smoothing it, (Figures 12(b) and 12(c)). Prewitt mask presents the worst result with the salt & pepper noise compared to other edges detectors because it does the averaging of neighbouring pixels. Since the salt & pepper noise pixel values are often different from the surrounding values, they tend to distort the computed

FIGURE 11. Test image corrupted by salt & pepper noise with density $d = 0.01$

(a) Gradient mask (b) Prewitt mask (c) Canny filter (d) N1OD ($K_1 = 400$)

FIGURE 12. Edge detection of the test image corrupted by salt & pepper noise

FIGURE 13. Test image corrupted by speckle noise with $\sigma_{ns} = 0.01$

average pixel. The performance of the Canny filter depends heavily on the adjustable parameter δ.

Tests with speckle noise. For Tables 1, 2 and 3, it has been noticed that for the Gaussian noise, the Canny filter presented the lowest value of the MEE. It is important to note that the obtained results can be improved by changing the thresholding method already used. Then the MEE depends strongly on the chosen of the threshold, and then it is more appropriate to consider the second indicator MME. From the MME values, N1OD performance is better for images corrupted with salt & pepper of noise compared to Gaussian or speckle noise.

Table 4 summarizes the elapsed time of the presented methods for different sizes of the frame. From these results, the proposed algorithms take more times to compute the gradient or Laplacian compared to other methods. This is due to the used computation method which is done pixel by pixel.

In Figure 15, the impact of the salt & pepper noise on the image "Lena" is often described of the true frame and the recorded one for each method. Figures 15(e) and 15(f) show the importance of the chosen of convergence gain of N1OD on the rate of

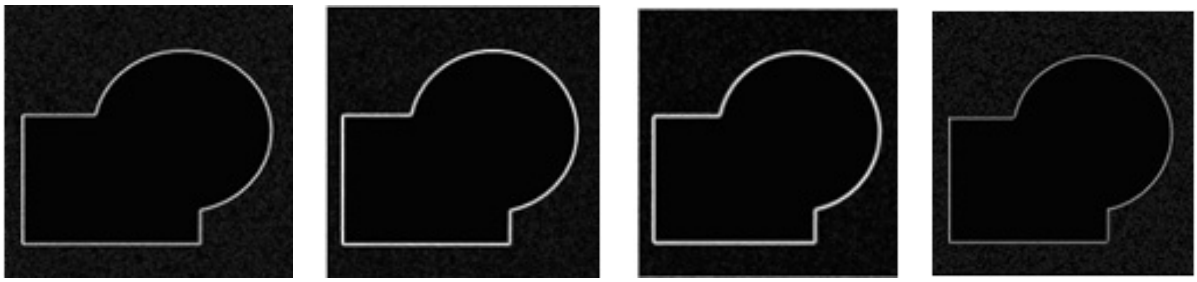

(a) Gradient mask (b) Prewitt mask (c) Canny filter (d) N1OD ($K_1 = 400$)

FIGURE 14. Edge detection of the corrupted image by speckle noise

TABLE 4. Elapsed time (s) for different sizes of image

Method	$(50 * 50)$	$(125 * 125)$	$(256 * 256)$
Gradient mask	0.00057	0.0017	0.0098
Prewitt mask	0.0011	0.0023	0.0040
Canny filter	0.0043	0.0064	0.0150
N1OD	0.0410	0.2556	1.0863
Laplacian operator	0.009	0.0138	0.0166
N2OD	0.0624	0.3930	1.6825

(a) Image 1 corrupted by salt (b) Gradient mask (c) Prewitt mask

(d) Canny filter (e) N1OD ($K_1 = 650$) (f) N1OD ($K_1 = 350$)

FIGURE 15. Edge detection of the corrupted "Lena" image by the salt & pepper noise

amplification noise in the resulted image. Indeed, increasing the value of the gain K_1, the amplification noise decreases.

In Table 5, some criteria for comparing the studied methods are presented. Despite good results provided by the proposed algorithms, it is essential to propose a solution to reduce their computation time in their discrete forms used for an image application.

TABLE 5. Criteria for comparing the studied edge detectors

Method	*Localization*	*Insensitivity to noise*	*Complexity of implementation*	*Computing time*	*Number of adjustment parameters*
Gradient mask	+	–	++	++	No parameters
Prewitt mask	+	+	++	++	No parameters
Canny filter	++	++	+	+	1
N1OD/N2OD	++	++	+	–	1/2

5. **Conclusions.** New higher order sliding modes differentiators are proposed and are well performed in order to extract the frame edge. Different simulation tests are presented in the 1D and 2D domains, where the efficacy of the proposed schemes is confirmed with comparing to the classic methods. In 1D domain and with noisy tests, a remarkable reduction of noise amplification is provided. In 2D domain, such algorithms work quite well for digital images corrupted with Gaussian noise, salt & pepper noise and the speckle noise. The results of this study are quite promising especially for video applications where the movement of a pixel can be estimated throughout the sequence. Other perspective to this work is the proposal of some solution to accelerate the computation time of the proposed algorithms.

REFERENCES

[1] A. M. Dabroom and H. K. Khalil, Discrete-time implementation of high-gain observers for numerical differentiation, *Int. J. of Control*, vol.72, no.17, pp.1523-1537, 1999.

[2] R. B. Brown and P. Y. C. Hwang, *Introduction to Random Signals and Applied Kalman Filtering*, 2nd Edition, John Wiley & Sons, 1992.

[3] J. E. Slotine and W. Li, *Applied Nonlinear Control*, Prentice-Hall, 1991.

[4] J. Davila, L. Fridman, A. Pisanob and E. Usaib, Finite-time state observation for non-linear uncertain systems via higher-order sliding modes, *Int. J. of Control*, vol.82, no.8, pp.1564-1574, 2009.

[5] L. Sidhom, M. Smaoui, D. Thomasset, X. Brun and E. Bideaux, Adaptive higher order sliding modes for two-dimensional derivative estimation, *The 18th World Congress of the Int. Federation of Automatic Control*, Milano, pp.3063-3071, 2011.

[6] M. Mboup, C. Join and M. Fliess, A revised look at numerical differentiation with an application to nonlinear feedback control, *The 15th Mediterrean Conf. on Control and Automation*, Athens, 2007.

[7] A. Levant, Higher order sliding modes, differentiation and output feedback control, *Int. J. of Control*, vol.76, pp.924-941, 2003.

[8] D. Marr and E. Hildreth, Theory of edge detection, *Proc. of the Royal Society of London*, vol.207, no.1167, pp.187-217, 1980.

[9] J. F. Canny, *Finding Edges and Lines in Images*, Massachusetts Inst. of Technology Cambridge, Artificial Intell. Laboratory, MA, USA, 1983.

[10] S. Riachy, Y. Bachalany, M. Mboup and J. P. Richard, An algebraic method for multi-dimensional derivative estimation, *The 16th IEEE Mediterranean Conf. on Control and Automation*, Ajaccio, 2008.

[11] A. Levant, Robust exact differentiation via sliding mode technique, *Automatica*, vol.34, no.3, pp.379-384, 1998.

[12] T. Uemura, G. Koutaki and K. Uchimura, Image segmentation based on edge detection using boundary code, *International Journal of Innovative Computing, Information and Control*, vol.7, no.10, pp.6073-6083, 2011.

[13] Q. Xu, S. Varadarajan, C. Chakrabarti and L. J. Karam, A distributed canny edge detector: Algorithm and FPGA implementation, *IEEE Trans. Image Process*, vol.23, no.7, pp.2944-2960, 2014.

[14] L. Sidhom, X. Brun, M. Smaoui, E. Bideaux and D. Thomasset, Dynamic gains differentiator for hydraulic system control, *J. of Dynamic Systems, Measurement, and Control*, vol.137, no.4, 2015.

Appendix A: Proof of Theorem 2.1. Let us define a quadratic Lyapunov function as follows:

$$V(\sigma) = \xi^T P \xi \tag{16}$$

with $\sigma = (\sigma_0, \sigma_1)^T$. At $t = 0$, let us note: $\sigma(t=0) = \sigma_{init} = (\sigma_0(0), \sigma_1(0))^T$. The vector ξ is chosen such that: $\xi = \begin{pmatrix} |\sigma_0|^{\frac{1}{2}} sign(\sigma_0) \\ \sigma_1 \end{pmatrix}$ where $P \in \mathbb{R}^{(2*2)}$ is a symmetric matrix given by:

$$P = \begin{pmatrix} 2\hat{\lambda}_1 + \frac{\Phi_0^2}{2} & -\frac{\Phi_0}{2} \\ -\frac{\Phi_0}{2} & 1 \end{pmatrix} \tag{17}$$

where $\Phi_0 = \hat{\lambda}_0 + K_0 |\sigma_0|^{\frac{1}{2}}$ is a positive quantity since $\hat{\lambda}_0 \geq 0$ and $K_0 \succ 0$. The matrix P is a positive definite matrix, since its eigenvalues $\bar{\lambda}_{1,2}$ are positive. Indeed, the characteristic equation of P is given by Equation (17) and with $\hat{\lambda}_1 \geq 0$, we can deduce that the eigenvalues of P are a positive real.

$$\bar{\lambda}^2 - \left(1 + 2\hat{\lambda}_1 + \frac{\Phi_0^2}{2}\right)\bar{\lambda} + 2\hat{\lambda}_1 + \frac{\Phi_0^2}{4} = 0 \tag{18}$$

Note that the defined Lyapunov function is continuous everywhere but not differentiable at $\sigma_0 = 0$. Here, $V(\sigma)$ is continuously differentiable, except on the set $S = \left\{(\sigma_0, \sigma_1) \in \mathrm{R}^{(2*2)} \middle| \sigma_0 = 0\right\}$, the Lyapunov theorem can only be applied to the points where $V(\sigma)$ is differentiable. Then, a non-smooth version of Lyapunov's theory is needed. Note that $V(\sigma)$ however positive definite and is bounded:

$$\bar{\lambda}_{\min}\{P\}\|\xi\|_2^2 \leq V \leq \bar{\lambda}_{\max}\{P\}\|\xi\|_2^2 \tag{19}$$

where $\|\xi\|$ is the Euclidean norm of ξ: $\|\xi\|_2^2 = |\sigma_0| + \sigma_1^2$. $\bar{\lambda}_{\min}\{P\}$, $\bar{\lambda}_{\max}\{P\}$ are respectively the minimum and maximum eigenvalues of the matrix P. The derivative of the vector ξ can be expressed as follows:

$$\dot{\xi} = |\sigma_0|^{-\frac{1}{2}} \begin{pmatrix} -\frac{\Phi_0}{2} & \frac{1}{2} \\ -\hat{\lambda}_1 & 0 \end{pmatrix} \xi = |\sigma_0|^{-\frac{1}{2}} A(\sigma)\xi \tag{20}$$

The time derivative of V along the system trajectories is then given by:

$$\dot{V} = |\sigma_0|^{-\frac{1}{2}} \xi^T \left(A^T(\sigma)P + PA(\sigma)\right)\xi = -|\sigma_0|^{-\frac{1}{2}} \xi^T Q(\sigma)\xi \tag{21}$$

where Q is:

$$Q = \frac{\Phi_0}{2} \begin{pmatrix} 2\hat{\lambda}_1 + \Phi_0^2 & -\Phi_0 \\ -\Phi_0 & 1 \end{pmatrix} \tag{22}$$

To conclude on the non-negativity of $\dot{V}$, the matrix Q has to be positively definite. From its characteristic equation (Equation (23)), we can deduce that the eigenvalues are positive and consequently that Q is positively definite:

$$\bar{\lambda}^2 - \left(1 + 2\hat{\lambda}_1 + \frac{\Phi_0^2}{2}\right)\bar{\lambda} + 2\hat{\lambda}_1 = 0 \tag{23}$$

From (23), we can write: $\|\xi\|_2 \leq \frac{V^{\frac{1}{2}}}{\bar{\lambda}_{\min}^{\frac{1}{2}}\{P\}}$.

Using Equations (17) and (23), we have:

$$|\sigma_0|^{\frac{1}{2}} \leq \left[|\sigma_0| + \sigma_1^2\right]^{\frac{1}{2}} \leq \frac{V^{\frac{1}{2}}}{\bar{\lambda}_{\min}^{\frac{1}{2}}\{P\}} \tag{24}$$

Therefore, we obtain:

$$\dot{V} \leq -\frac{\bar{\lambda}_{\min}^{\frac{1}{2}}\{P\}}{V^{\frac{1}{2}}}\bar{\lambda}_{\min}\{Q\}\|\xi\|_2^2 \tag{25}$$

Using the right inequality of the expression (17), (25) becomes:

$$\dot{V} \leq -\frac{\bar{\lambda}_{\min}^{\frac{1}{2}}\{P\}\bar{\lambda}_{\min}\{Q\}}{\bar{\lambda}_{\max}\{P\}}V^{\frac{1}{2}} = -\delta V^{\frac{1}{2}}, \text{ where } \delta = \frac{\bar{\lambda}_{\min}^{\frac{1}{2}}\{P\}\bar{\lambda}_{\min}\{Q\}}{\bar{\lambda}_{\max}\{P\}} > 0. \tag{26}$$

Let us consider now the general case of a differential equation of the following form:

$$\dot{\chi}(t) = -\delta\chi^{\frac{1}{2}}(t), \quad \chi(0) = \chi_0 \geq 0 \tag{27}$$

The solution of this equation is given by:

$$\int_0^t \frac{\dot{\chi}}{\chi^{\frac{1}{2}}}dt = -\int_0^t \delta dt \Rightarrow \chi(t) = \left(\chi_0^{\frac{1}{2}} - \frac{\delta}{2}t\right)^2 \tag{28}$$

From (28), $\chi(t)$ is equal to zero at a time t^* given by: $t^* = \frac{2\chi_0^{\frac{1}{2}}}{\delta}$. Then, it follows that $V(\sigma(t))$ and $\sigma(t)$ converge to zero in a finite time T given by: $T = \frac{2V^{\frac{1}{2}}(\sigma_{init})}{\delta}$.

Appendix B: Proof of Theorem 2.2. Let $\sigma_0 = s_0 = z_0 - f$. With this change of coordinate, the two first equations of system (8) can be written as follows:

$$\dot{\sigma}_0 = -\hat{\lambda}_0 \left|\sigma_0\right|^{\frac{2}{3}} sign\left(\sigma_0\right) - K_0\sigma_0 + \sigma_1 \tag{29}$$

where $\sigma_1 = z_1 - \dot{f}$. Since $\hat{\lambda}_0 \succ 0$ and $K_0 \succ 0$, from (29) we have:

$$\sigma_1 - \dot{\sigma}_0 = sign\left(\sigma_0\right)\left[\hat{\lambda}_0 \left|\sigma_0\right|^{\frac{2}{3}} + K_0\left|\sigma_0\right|\right] \tag{30}$$

and we can conclude that: $sign\left(\sigma_1 - \dot{\sigma}_0\right) = sign\left(\sigma_0\right)$.

Subtracting $\dot{f}$ on both sides of the second equation in (8), we obtain:

$$v_0 - \dot{f} = -\hat{\lambda}_0 \left|\sigma_0\right|^{\frac{2}{3}} sign\left(\sigma_0\right) - K_0\sigma_0 + z_1 - \dot{f} \tag{31}$$

Substituting $\dot{f}$ by its expression (11) in (31), we have:

$$\dot{\sigma}_0 = -\tilde{\lambda}_0 \left|\sigma_0\right|^{\frac{2}{3}} sign\left(\sigma_0\right) - K_0\sigma_0 \tag{32}$$

with $\tilde{\lambda}_0 = \hat{\lambda}_0 - \lambda_0^*$, which is an error between the dynamic value of the gain and *a priori one*.

Considering now $\sigma_1 = z_1 - \dot{f}$, we obtain $s_1 = \sigma_1 - \dot{\sigma}_0$. By subtracting $\ddot{f}$ from both sides of the last equation in (8) and taking account of this change of variable, we have:

$$\dot{\sigma}_1 = -\tilde{\lambda}_1 \left|\sigma_1 - \dot{\sigma}_0\right|^{\frac{1}{2}} sign\left(\sigma_1 - \dot{\sigma}_0\right) - K_1\left(\sigma_1 - \dot{\sigma}_0\right) - \tilde{\lambda}_2 \int_0^t sign\left(\sigma_1 - \dot{\sigma}_0\right) dt \tag{33}$$

Let us define a Lyapunov function as:

$$V\left(\sigma_0, \sigma_1, \tilde{\lambda}_i\right) = \frac{1}{2}\sigma_0^2 + \frac{1}{2}\left(\sigma_1 - \dot{\sigma}_0\right)^2 + \frac{1}{2}\sum_{i=0}^{2}\tilde{\lambda}_i^2, \quad i \in \{0,1,2\} \tag{34}$$

The equilibrium point is defined by $X_e^{\sigma,\tilde{\lambda}} = (0,0,0)$.

The derivative of this Lyapunov function is given by:

$$\dot{V} = \sigma_0\dot{\sigma}_0 + \left(\sigma_1 - \dot{\sigma}_0\right)\left(\dot{\sigma}_1 - \ddot{\sigma}_0\right) + \tilde{\lambda}_0\dot{\tilde{\lambda}}_0 + \tilde{\lambda}_1\dot{\tilde{\lambda}}_1 + \tilde{\lambda}_2\dot{\tilde{\lambda}}_2 \tag{35}$$

Then $\sigma_0\dot{\sigma}_0 + \tilde{\lambda}_0\dot{\tilde{\lambda}}_0 = -K_0\sigma_0^2$ and $(\sigma_1 - \dot{\sigma}_0)\dot{\sigma}_1 + \tilde{\lambda}_1\dot{\tilde{\lambda}}_1 + \tilde{\lambda}_2\dot{\tilde{\lambda}}_2 = -K_1(\sigma_1 - \dot{\sigma}_0)^2$. So, we have,

$$\dot{V} = -K_0\sigma_0^2 - K_1(\sigma_1 - \dot{\sigma}_0)^2 - (\sigma_1 - \dot{\sigma}_0)\ddot{\sigma}_0 \tag{36}$$

We have

$$-(\sigma_1 - \dot{\sigma}_0)\ddot{\sigma}_0 = -(\sigma_1 - \dot{\sigma}_0)\left[-\dot{\tilde{\lambda}}_0|\sigma_0|^{\frac{2}{3}}sign(\sigma_0) - K_0\dot{\sigma}_0 - \frac{2}{3}\tilde{\lambda}_0|\sigma_0|^{-\frac{1}{3}}\dot{\sigma}_0\right] \tag{37}$$

By introducing the dynamic gain $\hat{\lambda}_0$ (see system (10)) in (37), the following equality is satisfied:

$$-(\sigma_1 - \dot{\sigma}_0)\ddot{\sigma}_0 = -|\sigma_1 - \dot{\sigma}_0|\left[-|\sigma_0|^{\frac{7}{9}} + K_0^2|\sigma_0| + \frac{2}{3}\tilde{\lambda}_0^2|\sigma_0|^{\frac{1}{9}} + \frac{5}{3}\tilde{\lambda}_0K_0|\sigma_0|^{\frac{2}{9}}\right] \tag{38}$$

Consequently, Equation (38) can be rewritten as follows:

$$\begin{aligned}\dot{V} = & -K_0\sigma_0^2 - K_1(\sigma_1 - \dot{\sigma}_0)^2 - \frac{2}{3}|\sigma_1 - \dot{\sigma}_0|\tilde{\lambda}_0^2|\sigma_0|^{\frac{1}{9}} \\ & - |\sigma_1 - \dot{\sigma}_0|\left[-|\sigma_0|^{\frac{7}{9}} + \frac{5}{3}\tilde{\lambda}_0K_0|\sigma_0|^{\frac{2}{9}} + K_0^2|\sigma_0|\right]\end{aligned}$$

To show that $\dot{V}$ is negative, it is sufficient to prove that:

$$\Upsilon = \left[-|\sigma_0|^{\frac{7}{9}} + \frac{5}{3}\tilde{\lambda}_0K_0|\sigma_0|^{\frac{2}{9}} + K_0^2|\sigma_0|\right] \geq 0 \tag{39}$$

Therefore, let us assume that, $\left|\tilde{\lambda}_0\right| \leq \tilde{\lambda}_{0M}$ where $\tilde{\lambda}_{0M}$ is a positive constant satisfying the following inequality: $\tilde{\lambda}_{0M} < \frac{3}{5}K_0|\sigma_0|^{\frac{1}{3}}$.

In order to obtain the condition defined by (38), one must choose K_0 such that:

$$K_0\left[\tilde{\lambda}_0 + \frac{3}{5}K_0|\sigma_0|^{\frac{1}{3}}\right] \geq \frac{3}{5}|\sigma_0|^{\frac{5}{3}} \tag{40}$$

It is obvious that it is always possible to find some value of K_0 (namely a high-value) satisfying both inequalities (39) and (40).